Supporting Information

Dual-Functional Perylene Diimide Derivative for Efficient Organic Solar Cells and Interfacial Solar Steam Generation

Xiaolan Qin[a], Feilong Xia[b], Zhihao Liang[c], Junbo Chen[c], Zhuo Wang[a], Xiaxia Yang[c], Yuanpeng Xie[a*], Menglan Lv[a*]

[a] School of Chemistry and Chemical Engineering, Guizhou University, Guiyang, 550025 China

[b] Guizhou Wengfu Lantian Fluorchem Co., Ltd., Guiyang, 550025 China

[c] College of Materials and Metallurgy, Guizhou University, Guiyang, 550025 China

[*]Corresponding authors (Email: mllv@gzu.edu.cn, ypxie@gzu.edu.cn)

Characterizations

The UV-vis absorption spectra of PDIN-OH and PDIN in both solution and solid-state were characterized using a UV-vis-NIR spectrophotometer (Shimadzu UV3600, Japan). HOMO and LUMO energy levels of PDIN-OH determined via cyclic voltammetry. (GAMRY). The UPS measurements were performed by Thermo Fisher with He I as source gun type. (Thermo SCIENTIFIC Nexsa). Fluorescence spectra and fluorescence quantum efficiency tests were carried out on a steady-state and transient fluorescence spectrometer (Shimadzu RF-6000). The morphology of the samples was measured by a scanning electron microscope (SEM, Regulus 8100, JEOL, Japan). The transmission electron microscopy (TEM) images were obtained from Talos F200i microscope (Thermo Fisher Scientific, Czech Republic). The contact angles were probed with a contact angle measurement machine (JC2000D1, POWEREACH, China). Infrared images of the evaporator were captured using an infrared camera (DS-2TP21B-6AVF/ W, Hikvision, China). The evaporation behavior of water in CNH was observed by a differential scanning calorimeter (DSC) (TAQ2000, USA). The concentrations of irons (K^+, Ca^{2+}, Na^+, and Mg^{2+}) were measured using inductively couple plasma optical emission spectrometry (ICP-OES, Agilent 5110 (OES), USA).

Device fabrication and measurements

The patterned indium tin oxide (ITO) coated glass substrates (15 Ω per square) were successively cleaned by ultrasonic treatment in detergent, de-ionized and isopropanol, respectively. The cleaned ITO substrates were further dried by high purity nitrogen and treated by oxygen plasma for 100 s to improve their work function and clearance. Then, a 0.3 mg ml-1 solution of 4PAThCz was spin-coated at 3000 rpm onto a clean ITO glass, and roasted at 120 °C for 3 minutes. Before this, the D18:H8 and D18:L8-BO (1:1.2, weight ratio) blend had been dissolved in chloroform and stirred 2 hours at room temperature with a concentration of 4.5 mg·mL-1. Subsequently, these blend films were thermally annealed at 100 °C for 7 min after spin-coated at 2200 rpm. Later on, PDIN-OH and PDIN (as CILs) were deposited onto the active layers at 4200 rpm for 35 s from their solutions in methanol (1.2 mg·mL-1), respectively. Finally, Ag

(100 nm) electrode was thermally evaporated under 5×10-5 Pa and the device area was 0.0315 cm2 defined by shadow mask.

Calculation of the photothermal conversion efficiency

Based on previous reports,[1-3] the photothermal conversion efficiency of the photothermal conversion material was calculated with the following equation:

$$\eta = \frac{Q_a}{Q_s} \qquad (1)$$

Where Qa stands for the thermal energy generated, and Qs stands for the thermal energy generated.

$$Q_a = Cm\Delta T \qquad (2)$$

Where C, m, ΔT refer to heat capacity, quality and temperature difference of the solution, respectively.

$$Q_s = PSt \qquad (3)$$

Where Qs is determined by the power (P) of the incident light, the irradiation area (S) and irradiation time (t).

In this experiment, the specific heat capacities (C) of PDIN and PDIN-OH, measured by DSC, are 1157 J g^{-1} °C^{-1} and 1125 J g^{-1} °C^{-1} respectively, with both having an irradiation area of 2.25 cm^2. The relevant parameters and calculation results are as follows:

Table S1. Parameters related to calculating photothermal conversion efficiency.

sample	T_1 [°C]	T_2 [°C]	ΔT [°C]	t [s]	m[g]	Q_a [kJ]	Q_s [kJ]	η	$\bar{\eta}$
PDIN	27.0	39.8	12.8	4.5	0.044	0.6514	0.9	72%	67%
	36.2	39.7	3.5	2.0		0.1781	0.4	45%	
	28.9	40.0	11.1	3.4		0.5649	0.68	67%	
PDIN-	26.1	40.0	13.9	3.5	0.043	0.6648	0.7	95%	93%
OH	26.4	40.0	13.6	3.5		0.6504	0.7	93%	
	26.7	40.0	13.3	3.5		0.6361	0.7	91%	

DSC Test Method for Measuring Enthalpy of water Evaporation.

The test uses the DSC direct test method. First, the photothermal material was placed in an aluminum crucible, and heated from 0 °C to 180 °C in a nitrogen flow (50 mL min^{-1}) with a heating rate of 5 °C min^{-1}. Subsequently, the obtained DSC curves were plotted based on time and heat flow data, and the enthalpy of vaporization of the photothermal material was derived by integrating the peak areas of the resulting curves.

DSC measurement of energy consumption for water evaporation

The energy for water evaporation in the dark is obtained from the environment, which is same for different evaporators. E_{equ} and E_0 denote the equivalent evaporation enthalpy of water in the evaporator and the evaporation enthalpy of bulk water, respectively. m_0 represents the evaporation flux of bulk water under dark conditions, while mg is the evaporation flux in the evaporator under the same conditions.[4, 5]

$$U_{in} = E_{equ} m_g = E_0 m_0 \qquad (4)$$

Calculation of the efficiency for solar to vapor generation:

Efficiency η of solar energy in photothermal assisted water evaporation was calculated as the following formula.[6-8]

$$\eta = \frac{\Delta m E_{equ}}{P_{in}} \qquad (5)$$

Where Δm is the value obtained by subtracting the dark evaporation rate from the evaporation flux under illumination; E_{equ} is the evaporation enthalpy; and P_{in} (1 kW m^{-2}) is the irradiance of solar power.

$$\Delta m = m_{light} - m_{dark} \qquad (6)$$

Here, Equation (7) is equivalent to Equation (4).

$$E_{equ} m_g = E_0 m_0 \qquad (7)$$

Thus, the evaporation efficiencies of PDIN-OH, PDIN and Agel can be calculated as follows:

$$\eta_{PDIN-OH} = 94.95\%$$

$$\eta_{PDIN} = 73.6\%$$

Thermal conductivity characterization:

The thermal conductivity of the hydrogel was determined using the heat source method. The hydrogel was supported on both sides by PS foam and placed between two 10 mm thick glass plates, The system was placed on a copper plate continuously heated by a stable heat source. The thermal conductivity of PCs is calculated using the Fourier equation[9]:

$$q'' = k\frac{dT}{dx} \qquad (8)$$

Where q " is the heat flux, and dT/dx is the temperature gradient of the section in the vertical direction.

When the system reaches a steady state, use equation (2) to calculate the thermal conductivity of the PCs.

$$k_g\frac{dT_1}{dl_1} = k\frac{dT_2}{dl_2} \qquad (9)$$

In this context, kg and k correspond to the thermal conductivity of glass (1.05 W m^{-1} K^{-1}) and the thermal conductivity of the film, respectively. dT_1 and dT_2 represent the temperature differences across the upper and lower surfaces of the glass and the membrane, respectively. l_1 and l_2 are the thickness of the glass and sample, respectively.[10]

Supplementary Fig.s:

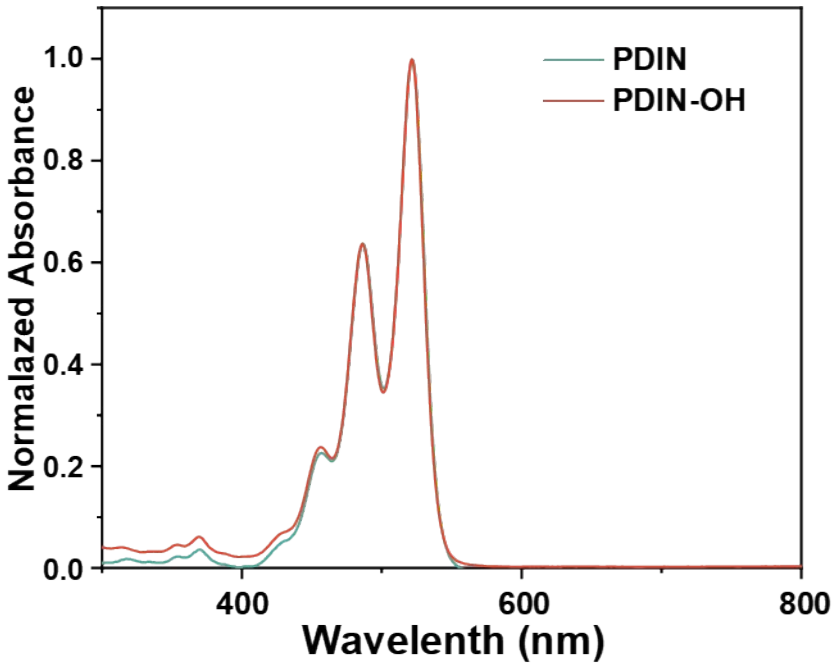

Fig. S1. UV absorption spectra of dilute solutions.

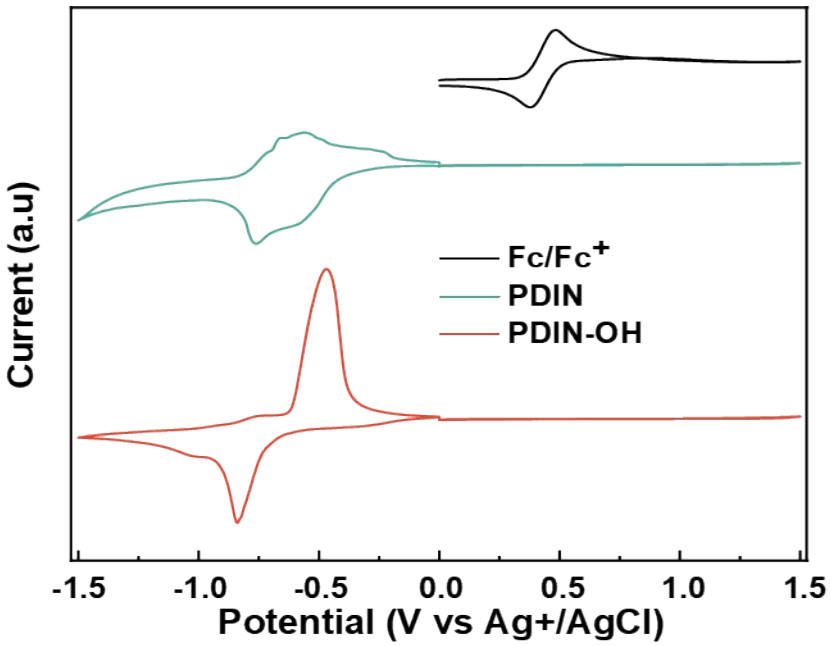

Fig. S2. Cyclic voltammograms of PDIN and PDIN-OH films in acetonitrile solution

Table S2. The performance with PDIN and PDIN-OH.

ETLs	Active layer	V_{OC} [V]	J_{SC} [mA cm^{-2}]	FF [%]	PCE [%]
PDIN	D18:H8	0.872	27.28	80.28	19.09
		0.873	27.26	79.99	19.02
		0.870	27.15	79.96	18.88
		0.868	27.08	80.56	18.94
		0.871	27.09	80.56	19.01
	D18:L8-BO	0.905	26.87	81.14	19.72
		0.896	26.98	80.36	19.43
		0.894	26.82	81.79	19.61
		0.890	26.72	81.97	19.49
		0.890	26.83	81.08	19.36
PDIN-OH	D18:H8	0.882	27.48	81.96	19.87
		0.882	27.33	81.52	19.64
		0.876	27.52	81.61	19.68
		0.885	27.53	81.49	19.85
		0.879	27.51	81.77	19.76
	D18:L8-BO	0.907	26.84	82.48	20.08
		0.904	26.94	82.98	20.21
		0.905	27.08	82.60	20.25
		0.903	27.10	82.29	20.14
		0.901	26.90	82.27	19.94

Table S3. The statistic of the device parameters of OSCs modified by typical PDI-derived non-ionic small molecule CILs reported since 2020.

CIL	Active layers	V_{OC}（V）	J_{SC} (mA cm^{-2})	FF (%)	PCE (%)	Date	Ref
PMI-TPP	PBDB-T:ITIC	0.88	17.55	68.00	10.42	2020	[11]
PDINN	PM6:Y6	0.85	25.89	78.59	16.77	2020	[12]
PDI-A	PTB7-Th:PC71BM	16.34	0.75	63.00	7.81	2021	[13]
PDI-Y	PTB7-Th:PC71BM	0.80	17.57	0.70	9.95	2021	[13]
PDIN	PM6:Y6	0.85	25.81	72.48	16.31	2021	[14]
PDI-M	D18Cl:Y6	0.86	26.28	76.18	17.41	2021	[14]
PDI-M	PM6:BTP-eC9	0.85	26.91	76.97	17.79	2021	[14]
PDI-M	PM6:Y6	0.85	74.41	26.14	17.98	2021	[14]
PDI-N	PM6:Y6	0.74	26.57	54.6	10.73	2022	[15]
PDIN-H/CC c	PM6:Y6	0.85	22.8	61.00	11.8	2022	[16]
CN-PDIN-H	PM6:Y6	0.85	22.7	63.00	12.2	2022	[16]
N-PDI8	PM6:Y6	0.84	23.80	60.00	12.5	2022	[17]
N-PDI18	PM6:Y6	0.84	23.8	60.00	11.9	2022	[17]
PDI-OSi	PM6:Y6	0.81	27.7	62.70	13.99	2022	[15]
2N-PDI	PM6:Y6BO	0.84	23.38	67.79	13.30	2023	[18]
PDIN-OTs	PM6:Y6BO	0.82	25.7	67.40	14.2	2023	[19]
PDINN-S	PM6:Y6	0.84	26.38	73.43	16.18	2023	[20]
H75	D18:Y6	0.85	27.11	79.03	18.26	2023	[21]
PDINN	PM6:Y6	0.84	25.55	74.35	15.96	2024	[22]
PDI-Br-1O	D18:EH-HD-4F	0.83	26.52	75.05	16.63	2024	[23]
PDI-Br-3O	D18:EH-HD-4F	0.84	27.24	78.12	18.10	2024	[23]
PDINN-TS	PM6:BTP-eC9	0.86	27.03	75.32	17.51	2024	[24]
PDINN-BS	PM6:BTP-eC9	0.86	27.27	76.84	18.02	2024	[24]
PDINN-2Br	PM6:PYIT	0.93	25.44	76.31	18.14	2024	[22]
CIL-ph	D18:L8-BO	0.92	26.23	77.55	18.43	2024	[25]
CIL-cp	D18:L8-BO	0.92	26.61	79.25	19.31	2024	[25]
PDI-OEG	PM6:L8-BO	0.90	26.81	0.78	18.72	2025	[26]
PDINBr	D18:L8-BO	0.91	26.48	75.18	18.29	2025	[27]
PDINBrCN	D18:L8-BO	0.90	26.67	77.68	18.83	2025	[27]
PDI-Leu-am	D18:L8-BO	0.91	27.10	79.83	19.75	2025	[28]
PDINN-B2F	PM6:L8-BO	0.87	26.56	76.99	17.79	2025	[29]
PDINN-B3F	PM6:L8-BO	0.88	26.78	77.99	18.38	2025	[29]
PDI-P	PM6: BTP-eC9	0.865	28.6	80.0	19.80	2025	[30]

P-C3T	D18:L8-BO	0.922	26.45	79.73	19.52	2025	[31]
PDIN-OH	D18:L8-BO	0.905	27.08	82.60	20.25	2025	**This work**

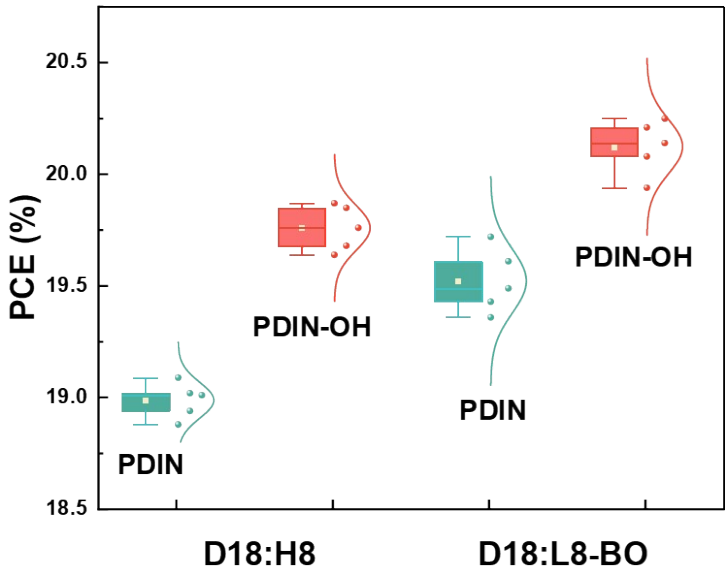

Fig. S3. The statistic of PCEs based on various ETL and active layers.

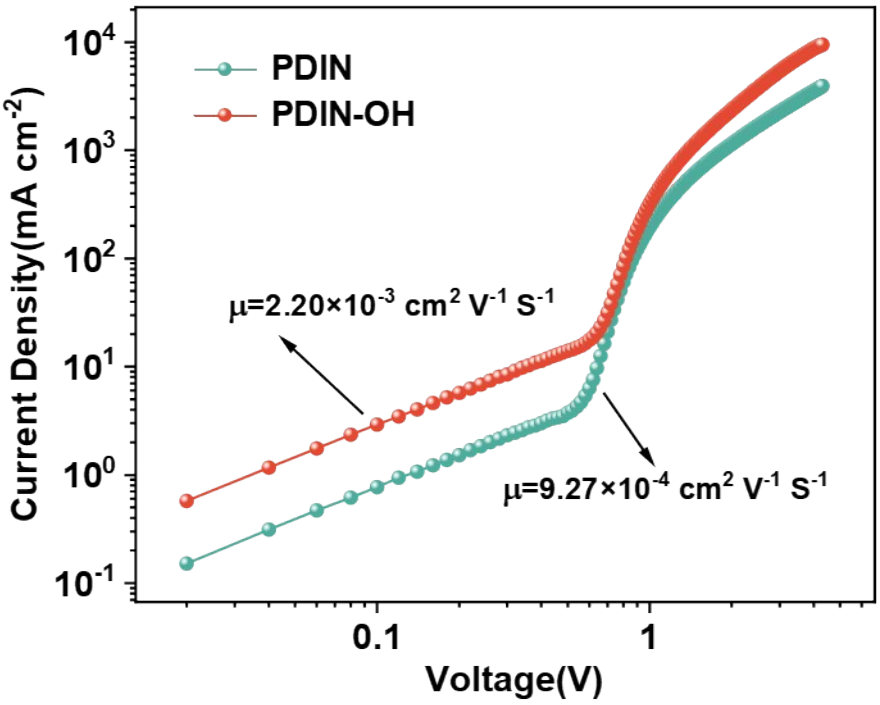

Fig. S4. VTFL of devices.

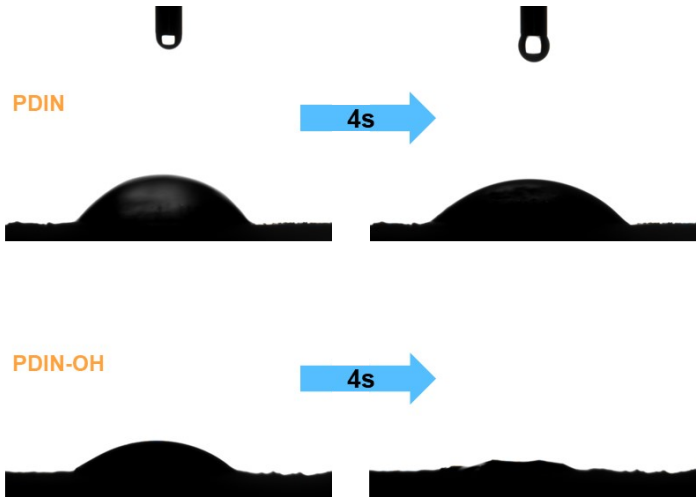

Fig. S5 The contact angle measurement of PDIN and PDIN-OH.

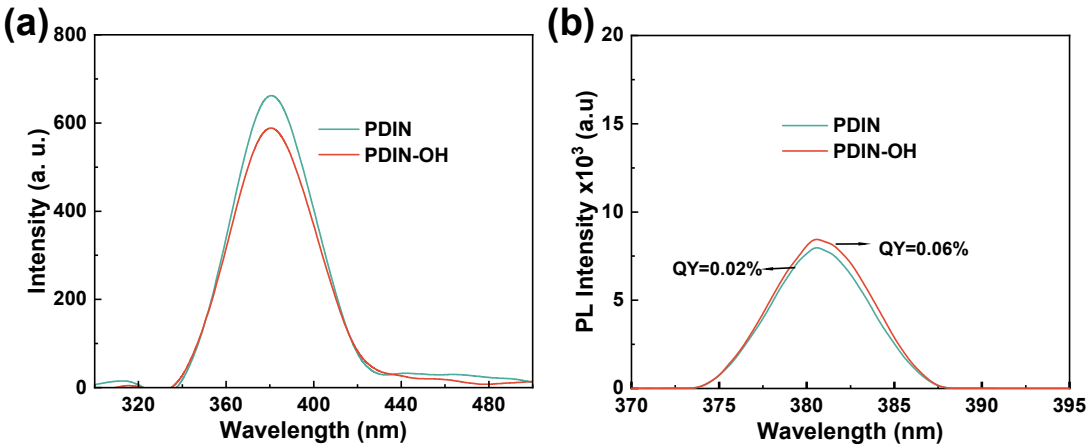

Fig. S6. (a) Fluorescence spectra of PDIN and PDIN-OH in the solid state, (b) Photoluminescence (PL) intensity spectra of PDIN and PDIN-OH in powder form.

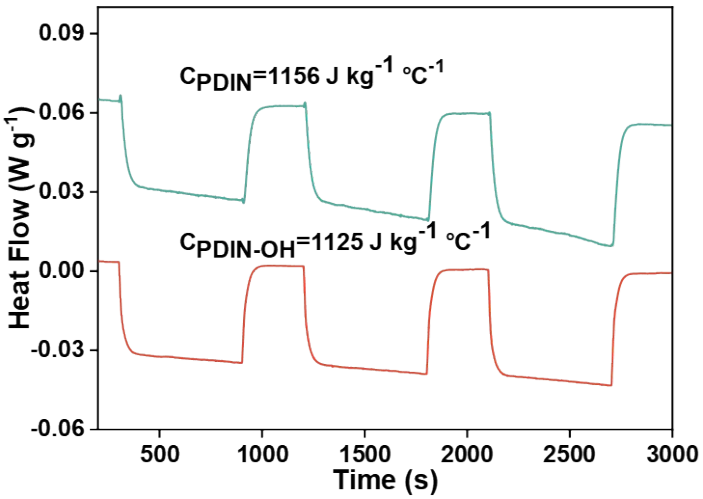

Fig. S7. Differential scanning calorimetry (DSC) profiles of PDIN-OH and PDIN.

Fig. S8. Photograph of an elasticity test of hydrogel.

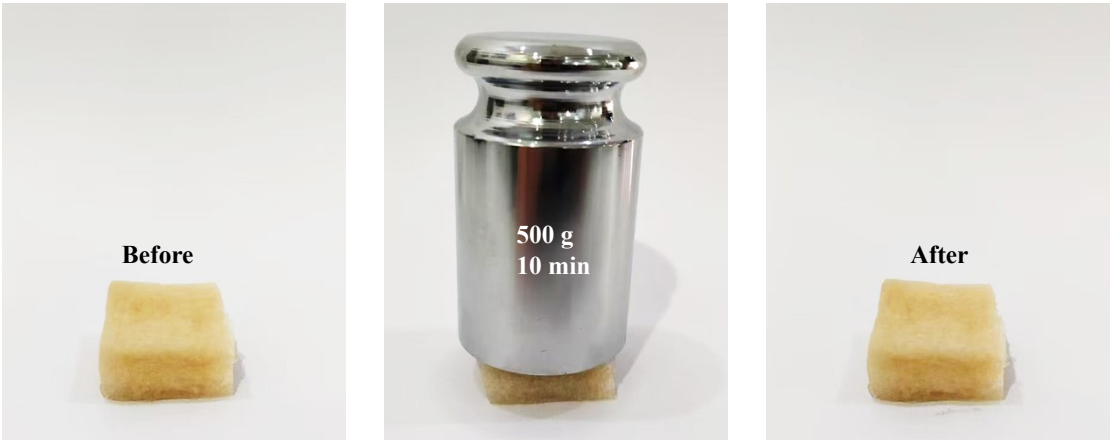

Fig. S9. Comparison of hydrogel before and after bearing a 500 g weight.

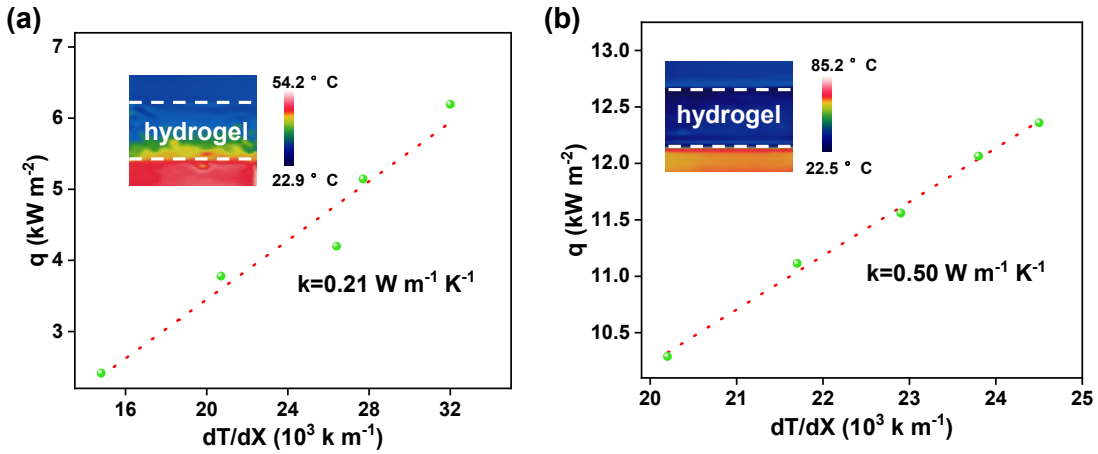

Fig. S10. (a) Thermal conductivity of the hydrogel under drying, and (b) thermal conductivity of the hydrogel in the wet state.

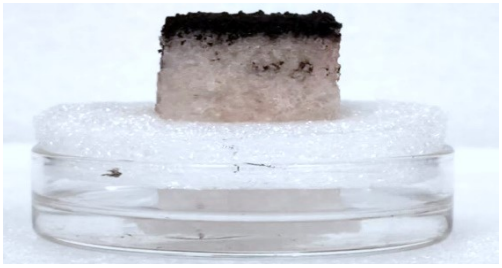

Fig. S11. Photograph of the solar evaporator during outdoor testing.

Table S4. Comparison of our Results with representative parameters of small organic molecular photothermal materials in ISSG from recent literature.

Photothermal conversion material	photothermal conversion efficiency	evaporation efficiency	Evaporation rate （kg m^{-2} h^{-1}）	year	Ref
CR-TPE-T	72.7%，	87.20%	1.272	2020	[32]
DDPA-PDN	56.23%	73.98	1.07	2021	[33]
TPP-2 IND	-	65.80%	1.04	2023	[34]
PDI-DTMA	20.60%	-	3.61–10.07	2023	[35]
CFO/PDA@ MF	-	89%	2.03	2024	[36]
T-TTD-T	65.50%	85.20%	1.24	2024	[37]
TPA-SBTQ	18.28%	92%	1.337	2024	[38]
PRF/GGSM	92%	-	3.8	2024	[39]
UiO-PDIc	-	99%	1.44	2025	[40]
PDI/GGrS	90%	57%	3.5	2025	[41]
PDIN-OH	93%	95%-	3.7	2025	**This work**

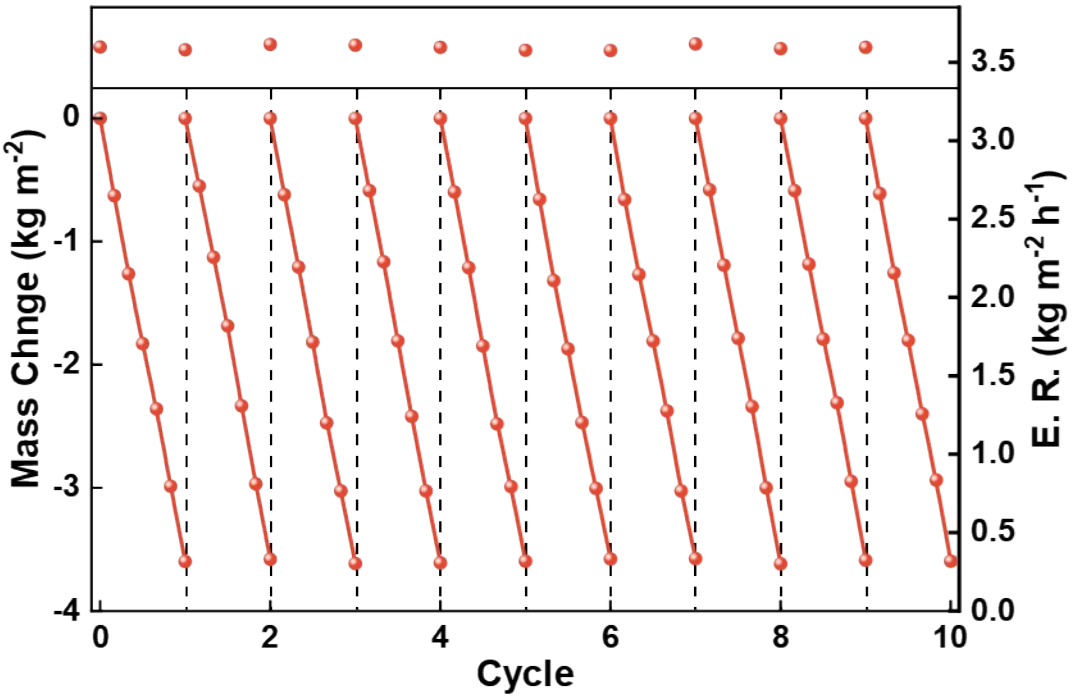

Fig. S12. Cycle stability in solar steam power generation.

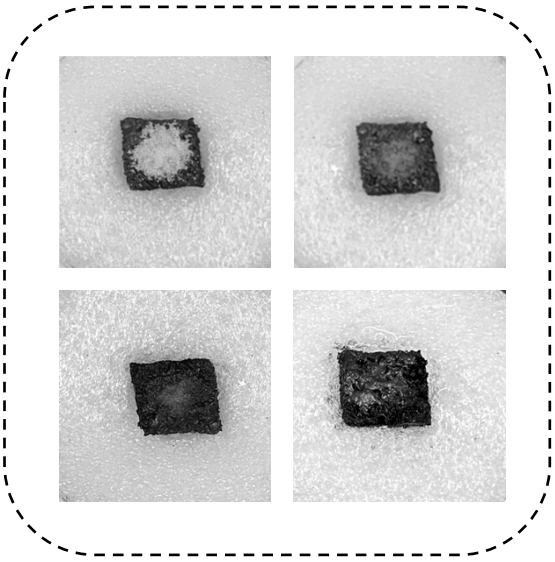

Fig. S13. Dissolution behavior of 1 g salt on the surface of PDIN-OH under illumination.

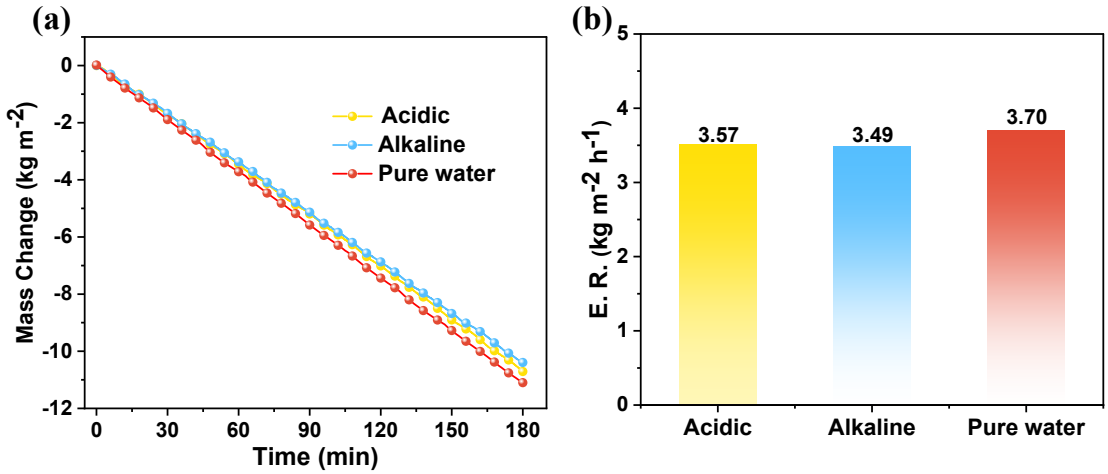

Fig. S14 (a) The mass change of water in the PDIN-OH evaporator under standard irradiation (1 kW·m⁻²) was measured in environments with pH values of 3, 7, and 11, respectively; (b) The evaporation rate of the PDIN-OH evaporator in environments with pH values of 3, 7, and 11, respectively.

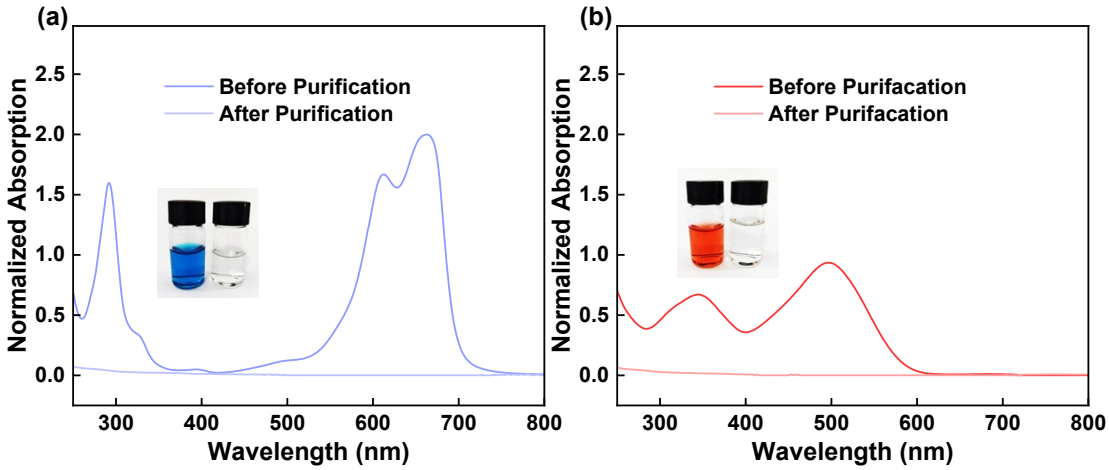

Fig. S15. (a) UV-Vis absorption spectra of organic wastewater containing methylene blue before and after purification; (b) UV-Vis absorption spectra of organic wastewater containing rhodamine B before and after purification. The insets are water samples.

Supplemental References

1. P. Zhang, J. Li, L. Lv, Y. Zhao and L. Qu, *Acs Nano*, 2017, **11**, 5087-5093.
2. Z. Li, X. Xu, W. Zhang, X. Meng, Z. Genene, W. Ma, W. Mammo, A. Yartsev, M. R. Andersson, R. A. J. Janssen and E. Wang, *Energy Environ. Sci.*, 2017, **10**, 2212-2221.
3. M. Zhao, Y. Zhu, Y. Pan, Y. Wang, T. Xu, X. Zhao, T. Jia, Z. Zhang and Z. Chen, *ACS Appl. Energ. Mater.*, 2022, **5**, 15758-15767.
4. Y. Guo, H. Lu, F. Zhao, X. Zhou, W. Shi and G. Yu, *Advanced Materials*, 2020, **32**, 1907061.
5. G. Hu, H. Liu, K. Liu, H. Wang, X. Wen, L. Liu, Y. She, L. Feng, R. Niu and J. Gong, *Adv. Funct. Mater.*, 2025, **35**, 2423781.
6. C. Lei, W. Guan, Y. Guo, W. Shi, Y. Wang, K. P. Johnston and G. Yu, *Angewandte Chemie-International Edition*, 2022, **61**, e202208487.
7. M. Tian, H. Lu, H. Li, J. Tian, Y. Guo, X. Hu, H. Xie and H. Y. Xie, *Chem. Eng. J.*, 2024, **494**, 152940.
8. L. Zhou, Y. Tan, J. Wang, W. Xu, Y. Yuan, W. Cai, S. Zhu and J. Zhu, *Nat. Photonics*, 2016, **10**, 393-+.
9. H. Li, Y. He, Y. Hu and X. Wang, *ACS Appl. Mater. Interfaces.*, 2018, **10**, 9362-9368.
10. F. Li, N. Li, S. Wang, L. Qiao, L. Yu, P. Murto and X. Xu, *Adv. Funct. Mater.*, 2021, **31**, 2104464.
11. R. Qin, D. Guo, L. Hu, Z. Liu, J. Yang, H. Liu, L. Jiang and Y. Jiang, *Energy Technol.*, 2020, **8**, 2000072.
12. J. Yao, B. Qiu, Z.-G. Zhang, L. Xue, R. Wang, C. Zhang, S. Chen, Q. Zhou, C. Sun, C. Yang, M. Xiao, L. Meng and Y. Li, *Nat. Commun.*, 2020, **11**, 2726.
13. Y. O. Kim, B. J. Moon, A. Lee, J. I. Kim, S. K. Lee, Y. S. Lee, S. Bae, B. H. Hong and Y. C. Jung, *Adv. Opt. Mater.*, 2021, **9**, 2101006.
14. M. Liu, Y. Jiang, D. Liu, J. Wang, Z. Ren, T. P. Russell and Y. Liu, *ACS Energy Lett.*, 2021, **6**, 3228-3235.
15. D. Zhou, J. Quan, H. Zhang, H. Zheng, Z. Xu, F. Wang, L. Hu, J. Liu, Y. Tong

and L. Chen, *ACS Appl. Mater. Interfaces.*, 2022, **14**, 54063-54072.

16. M. E. Farahat, M. A. Anderson, M. Martell, E. L. Ratcliff and G. C. Welch, *ACS Appl. Mater. Interfaces.*, 2022, **14**, 43558-43567.
17. A. Hoff, M. Martell, A. Gasonoo, J. D. B. Koenig, P. Simón Marqués, E. Cieplechowicz, M. Pahlevani and G. C. Welch, *Adv. Eng. Mater.*, 2022, **25**, 2201437.
18. F. Pan, S. Bai, T. Liu, D. Tang, X. Wei, X. Chen, M. Lv and Y. Li, *Sci. China Chem.*, 2021, **64**, 565-575.
19. S. A. Salma, R. F. B. Nasrun, Q. A. K. Nisa, D. H. Son and J. H. Kim, *Dyes Pigment.*, 2023, **217**, 111345.
20. D. Zhou, L. Han, L. Hu, S. Yang, X. Shen, Y. Li, Y. Tong, F. Wang, Z. Li and L. Chen, *ACS Appl. Mater. Interfaces.*, 2023, **15**, 8367-8376.
21. T. L. H. Mai, S. Jeong, S. Kim, S. Jung, J. Oh, Z. Sun, J. Park, S. Lee, W. Kim and C. Yang, *Adv. Funct. Mater.*, 2023, **33**, 2303386.
22. K. Zhong, J. Deng, R. Zeng, J. Xu, Z. Yuan, C. Wang, L. Li, J. Liu, X. Zhao, Y. Hu, L. Chen and F. Liu, *Adv. Funct. Mater.*, 2025, **35**, 2414822.
23. L. Tian, L. Feng, S. Guo, R. Wang, K. Zhang and C.-X. Cui, *J. Mater. Chem. A*, 2024, **12**, 6644-6651.
24. S. Lan, D. Zhou, L. Hu, H. Li, Y. Pu, F. Wang, W. Wan, Y. Tong, R. Lv, H. Xu, B. Hu, P. Cheng, Z. Li and L. Chen, *Adv. Funct. Mater.*, 2024, **35**, 2419205.
25. H. Jiang, Q. Liang, H. Guo, A. Zhang, X. Wang, Z. Tang and Z. Bo, *J. Am. Chem. Soc.*, 2024, **146**, 30262-30271.
26. W. Xiao, Y. Xiang, Q. Li, Z. Li, B. Xu and S. Yan, *Small*, 2025, **21**, 2502094.
27. Y. Wang, X. Jiang, H. Song, N. Wei, Y. Wang, X. Xu, C. Li, H. Lu, Y. Liu and Z. Bo, *Acta Phys.-Chim. Sin.*, 2025, **41**, 100027.
28. X. Wang, Q. Liang, A. Zhang, N. Wei, H. Jiang, Y. Cheng, H. Fang, S. Li, H. Lu, W. Li and Z. Bo, *J. Am. Chem. Soc.*, 2025, **147**, 9261-9272.
29. L. Hu, J. Wang, F. Wang, G. Shen, H. Li, W. Li, Y. Jin, Z. Su, M. Du, J. Yao, Z. Yan, P. Cheng, D. Zhou, E. Zhou and Z. Li, *Adv. Funct. Mater.*, 2025, DOI:

10.1002/adfm.202520155.

30. Y. Li, L. Wang, H. Fu and Q. Zheng, *Adv. Funct. Mater.*, 2025, **35**, 2419342.
31. Y. Guo, X. Ma, H. Song, J. Chen, W. Zhang, X. Xu, C. Li, Y. Liu, Y. Liu and Z. Bo, *Adv. Funct. Mater.*, 2025, **35**, 2416356.
32. G. Chen, J. Sun, Q. Peng, Q. Sun, G. Wang, Y. Cai, X. Gu, Z. Shuai and B. Z. Tang, *Adv. Mater.*, 2020, **32**, 1908537.
33. Y. Cui, J. Liu, Z. Li, M. Ji, M. Zhao, M. Shen, X. Han, T. Jia, C. Li and Y. Wang, *Adv. Funct. Mater.*, 2021, **31**, 2106247.
34. J. C. Yang, L. Wu, L. Wang, R. Ren, P. Chen, C. Qi, H. T. Feng and B. Z. Tang, *Aggregate*, 2024, **5**, e535.
35. C. Shao, B. Guo, B. Lu, J. Yu, H. Kong, B. Wang, M. Ding and C. Li, *Small*, 2023, **19**, 2305856.
36. C. Cheng, H. Miao, Y. Chai, R. Yuan and H. Liu, *Acs Materials Letters*, 2023, **6**, 132-139.
37. L. Guo, X. Kong, R. Li, J. Sun, G. Wang and X. Gu, *Dyes Pigment.*, 2024, **227**, 112195.
38. L. Wang, H. Wang, S. Yu, N. An, Y. Pan, J. Li, T. Jia, K. Wang and W. Huang, *Adv. Funct. Mater.*, 2024, **34**, 2315762.
39. E. Erçarıkcı, D. Demirci Gültekin, E. Topçu, Z. Kudaş, M. Alanyalıoğlu and K. Dağcı Kıranşan, *ACS Appl. Mater. Interfaces.*, 2024, **16**, 61910-61920.
40. J. Wang, K. Mullen, J. Guan and M. Yin, *J. Mater. Chem. A*, 2025, **13**, 34804-34812.
41. E. Erçarıkcı, D. Demirci Gültekin, E. Topçu, Z. Kudaş, M. Alanyalıoğlu and K. Dağcı Kıranşan, *Desalination*, 2025, **593**, 118237.